Cation Siting and Dynamical Properties of Zeolite Offretite from First-Principles Molecular Dynamics

L. Campana,[†,‡] A. Selloni,[†] J. Weber,*[,†] and A. Goursot[§]

Department of Physical Chemistry, University of Geneva, 30 quai E. Ansermet, CH-1211 Geneva 4, Switzerland, Institute IRRMA, Swiss Federal Institute of Technology, PHB−Ecublens, CH-1015 Lausanne, Switzerland, and UMR 5618 CNRS, National School of Chemistry, 8 rue de l'Ecole Normale, F-34053 Montpellier, France

Received: April 3, 1997; In Final Form: July 17, 1997[⊗]

We have used density functional theory, both within the local density (LDA) and generalized gradient (GGA) approximations, to study the structure, energetics, and vibrational properties of zeolite offretite in the presence of different monovalent cations (H^+, Na^+, K^+, and Cu^+). We find that the spatial locations of the most favorable cation-binding sites are similar for the different cations, being related to the minima of the electrostatic potential. However, the relative stability of the sites does depend on the nature of the counterion, as well as on the Al/Si ratio and on the mutual interactions between cations. At low Al/Si ratios, the preferred site for H^+ is in the channel, where it is accessible for reaction with incoming molecules. For both Na^+ and Cu^+, the most stable site is within the 6-fold ring of the gmelinite cage, but for Na^+, two other sites are present within a few tenths of a kilocalorie/mole from the lowest site (small site selectivity). For K^+, two sites, one inside the cancrinite cage and the other near the 8-fold ring of the gmelinite cage, are very close in energy, consistent with the X-ray experiments on natural hydrated and dehydrated offretites. Dynamical simulations have been carried out for H− and Na−offretite. The vibrational spectrum of the framework agrees well with the available experiment. OH stretching frequencies calculated for a number of different H^+ locations show that more "open" positions, e.g., in the channel, have higher frequencies, in agreement with experiment.

I. Introduction

Knowledge of the cation distribution in zeolites is very important for understanding their activity.[1] The most widely used neutralizing counterions are protons, which are known to be firmly bonded to the lone pairs of the bridging oxygen species. These acidic hydroxyl groups play a crucial role in the catalytic activity of zeolites. As an alternative to proton counterions, monovalent (e.g., Na^+, K^+), divalent (eg., Ca^{2+}), or trivalent (e.g., La^{3+}) cations can be incorporated into extra-framework sites of the zeolite. These cations tend to be close to two or more oxygen atoms with which they form weak bonds, but their precise locations are frequently unknown.

In this paper, we present an extensive density functional study of the structure, energetics, and vibrational properties of zeolite offretite in the presence of several different monovalent cations (H^+, Na^+, K^+, and Cu^+). Our purpose is to identify and characterize the various cation sites, as well as to investigate how different properties depend on the nature of the counterion. Offretite is a quite rare zeolite, which has been mostly chosen because of its relatively low number of atoms per unit cell (54 atoms). Natural offretite usually has K^+, Ca^{2+}, and Mg^{2+} counterions (schematic formula: $KCaMgAl_5Si_{13}{\cdot}nH_2O$, where $n = 15-17$), with a smaller amount of Na^+ and other divalent ions.[2] Its structure has been studied experimentally by Gard and Tait[3] and more recently by Alberti *et al.*,[4] while dehydrated offretite was investigated by Mortier *et al.*[5] Offretite can be also synthesized, usually in the presence of TMA^+ and/or K^+ cations,[6,7] and different counterions, such as H^+, Li^+, and Cs^+, have been introduced via ion exchange. Although we are not aware of any experimental study of Cu^+ in offretite, we believe it is instructive to compare the behavior of a metal ion with 3d electrons such as Cu^+ to that of simple alkali metals. Moreover, the interaction of Cu^+ with zeolitic frameworks is of great current interest, due to the importance of Cu-ZSM-5 as a catalyst for NO_x reduction.[8]

The work presented in this paper is a continuation and extension of that described in our previous papers on protonated offretite[9] and offretite in the presence of Na^+ and K^+ conteri-ons.[10] New results are reported concerning the structure and energetics of various Cu^+ sites, the dynamical properties of offretite in the presence of Na^+ and H^+ counterions, and the influence of mutual cation−cation interactions and the Al/Si ratio on the cation distribution. As in our previous work, calculations have been carried out within the framework of the first-principles molecular dynamics (FPMD) approach developed by Car and Parrinello,[11] using a periodic lattice representation of offretite and allowing for full relaxation of all atomic positions. Here, however, we are not restricted to the local density approximation (LDA) of density functional theory but also present calculations performed with a gradient-corrected exchange-correlation functional, i.e., the so-called generalized gradient approximation (GGA) by Perdew and Wang.[12] This approximation has been extensively tested and shown to be significantly more accurate than the LDA at describing energetic properties, e.g., cohesive energies.[12,13] Moreover, the calculations presented in this paper, particularly those for protonated offretite, use a much larger basis set than that employed in our previous work. There are, therefore, some nonnegligible differences between the present and the previously published calculations, and the new results are typically in much better agreement with the available experimental information.

The layout of this paper is as follows. After a brief description of the model and of the computational details, we present our results for protonated offretite. We first discuss

[†] University of Geneva
[‡] Swiss Federal Institute of Technology.
[§] National School of Chemistry.
[⊗] Abstract published in *Advance ACS Abstracts,* October 15, 1997.

S1089-5647(97)01167-X CCC: $14.00

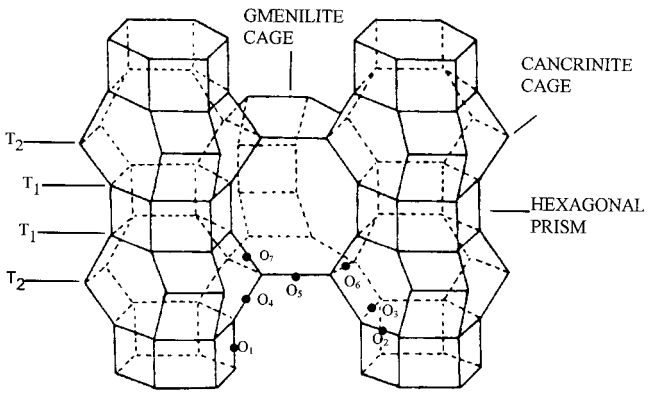

Figure 1. Framework structure of offretite. Vertices correspond to silicon or aluminum atoms at tetrahedral (T) sites. Inequivalent T sites and oxygen atoms are indicated, O_4 and O_7 become inequivalent when an Al is in T_1.

the structure and energies of different H^+ sites and next present the results of our dynamical simulations. These concern both the vibrational spectrum of the framework and the OH stretching frequencies for H^+ at different sites. The following section reports the results for K^+, Na^+, and Cu^+. Again, we first discuss static properties (cation siting) and next dynamical properties (in the presence of a Na^+ counterion). A third subsection is devoted to a study of cation siting in the case of higher Al/Si ratios and correspondingly higher cation concentrations. Finally, a brief summary and conclusions are given.

II. Computations

A. Geometry. Offretite is hexagonal, and its structure comprises three types of cavities: a cancrinite cage, a gmelinite cage, and a hexagonal prism (see Figure 1). These cages circumscribe large channels, parallel to the *c* axis, encompassed by 12 oxygens. The unit cell has 2 distinct tetrahedral (T) sites, namely, 12 T_1 sites, belonging to the hexagonal prisms, and 6 T_2 sites, in the 6-fold rings of the gmelinite cages. To investigate the substitution of silicon by aluminum at either T_1 or T_2, we considered a periodically repeated unit cell containing 36 oxygen, 17 silicon, 1 aluminum, and 1 M (M = H, Na, K, Cu) atoms. For a few calculations (see below), a unit cell containing 36 oxygen, 15 silicon, 3 aluminum, and 3 M atoms was also used. We have taken the unit cell dimensions $a = b = 13.291$ Å and $c = 7.582$ Å as given in ref 3 for hydrated offretite. For the structure containing only silicon, there are six nonequivalent oxygens (see Figure 1). It is important to notice that the labeling of oxygen sites used in this work (and in our previous papers[9,10]) is different from the conventional one (see refs 3−5). The correspondence between the two sets of labels is as follows:

conventional	this work
O_1	O_4
O_2	O_3
O_3	O_2
O_4	O_1
O_5	O_6
O_6	O_5

When the T_1 site is aluminated, the four oxygens bound to it are nonequivalent, whereas in the case of a T_2 site, this number is three as O_4 and O_7 (see Figure 1) are equivalent by symmetry.

B. Technical Details. Several detailed descriptions of the FPMD method are now available in the literature (see e.g., ref 14). Thus, in this section, we are restricted to a summary of the main technical ingredients of our calculations. The electronic valence wave functions have been expanded in plane waves and are calculated only at the Γ point of the Brillouin zone. For Si and Al, electron−core interactions are described by norm-conserving pseudopotentials[15] in a Kleinman and Bylander form,[16] whereas for oxygen, Na, K, and Cu "ultrasoft" pseudopotentials[17] were used. For Na (K), 2s and 2p (3s and 3p) shells have been treated as valence states in order to improve the transferability, while Cu valence states include 3d and 4s electrons. Pseudopotential cutoff radii were 1.5, 1.6, 1.9, and 2.0 au for O, Na, K, and Cu, respectively. A kinetic energy cutoff $E_{cut,1} = 20$ or 24 Ry has been used for the smooth part of the electronic wave functions (the latter is used for protonated offretite), while the cutoff for the augmented electron density was $E_{cut,2} = 200$ Ry.[18] The parametrisation of Perdew and Zunger[19] has been used for the local exchange-correlation functional, while the gradient-corrected exchange-correlation functional is taken from ref 12. GGA calculations were performed using LDA-optimized geometries and charge densities. This non-self-consistent approach to GGA calculations has been shown to yield energies that are usually in excellent agreement with fully self-consistent GGA calculations.[12,20] A preconditioned algorithm[21] was enabled us to increase the time step in the search of the electronic solution. With a preconditioning cutoff $E_p = 2$ Ry and an electronic fictitious mass $\mu = 700$ (500) au, our time step was $\Delta t = 15$ (10) au [=3.6 (2.4) × 10^{-16} s] in the case of K^+ (Na^+). The atom positions were relaxed using a damped second-order dynamics algorithm until residual forces were less than 0.0003 au. In dynamical simulations, carried out using the LDA, atomic masses were corrected using the formulas presented in ref 22.

III. Protonated Offretite

A. H^+ Siting and Acidity. As H^+ is known to be localized on a single oxygen, we have considered all configurations arising from the substitution of Si^{4+} by an Al^{3+} in a T_1 or T_2 site with a proton bonded to each nonequivalent oxygen of the AlO_4 tetrahedron. In this way, seven different structures are obtained, four for the case of Al in T_1 and three for Al in T_2. These have been fully optimized first using a relatively low energy cutoff, $E_{cut,1} = 16$ Ry (these results have been reported in ref 9), and subsequently increasing the cutoff to 24 Ry. These structures will be denoted as T_1O_jH and T_2O_jH ($j = 1-7$). The energies to substitute a Si^{4+} by (Al^{3+}, H^+) are calculated using the expression

$$E_{subs} = [E(T_iO_jH) + E_{Si}] - [E_{off} + E_{Al} + E_H]$$

where $E(T_iO_jH)$ is the energy of the structure T_iO_jH, E_{off} is the total energy of Al-free offretite, and E_{Si}, E_{Al}, and E_H are atomic energies.

The calculated substitution energies, both within the LDA and the GGA, are reported in Table 1. The differences between the two sets of results are of the order of 5 kcal/mol but do not alter the relative ordering of sites. From Table 1, it appears that two structures are significantly more stable than all the others. These two structures, which are energetically very close, should be the only sites occupied at room temperature. They correspond to H within the gmelinitic 6-fold ring (T_2O_6H) and to H in the channel (T_2O_7H). For both structures, Al is the T_2 site, suggesting a greater stability of this site. This is in agreement with the experiental finding that dealumination is easier in T_1 than in T_2.[23] Furthermore, in ref 4, a greater population of Al in T_2 than in T_1 was found.

The stability of T_2O_7H and T_2O_6H can be rationalized by considering the electrostatic potential $V_H(\mathbf{r})$ in the absence of the proton. Isovalue surfaces of $V_H(\mathbf{r})$ with an Al in T_2 and

TABLE 1: Substitution Energies (E_{subs}) and "Proton Affinities" (Δ, See Text) of Inequivalent Protonated Sites in Offretite (in kcal/mol)[a]

	LDA		GGA	
structure	E_{subs}	Δ	E_{subs}	Δ
T_1O_1H	−34.2 (7.0)	303.6	−39.0 (7.3)	309.4
T_1O_2H	−35.1 (6.0)	304.6	−38.0 (8.3)	308.4
T_1O_3H	−34.9 (6.2)	304.4	−38.8 (7.4)	309.3
T_1O_4H	−34.0 (7.1)	303.5	−38.7 (7.6)	309.2
T_2O_5H	−32.7 (8.5)	294.6	−37.0 (9.3)	299.7
T_2O_6H	−40.3 (0.9)	302.2	−45.0 (1.3)	307.7
T_2O_7H	−41.1 (0.0)	303.1	−46.3 (0.0)	309.0

[a] Values in parentheses are substitution energies relative to the most stable site. The estimated accuracy of relative quantities in 1 mH = 0.6 kcal/mol.

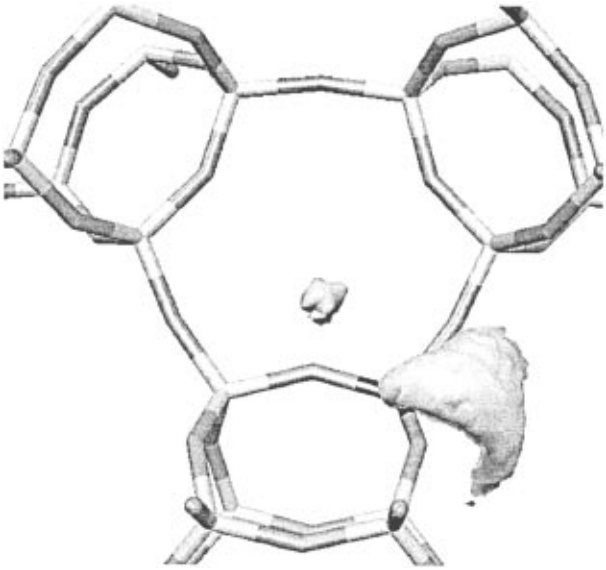

Figure 2. Isovalue surfaces of the electrostatic potential (−0.145 au) of offretite with an Al in T_2 and no counterion. All atoms within one unit cell are shown: light gray, dark gray, and black correspond to Si, O, and Al (partially hidden), respectively. The smaller pocket is in proximity to T_2O_6H; the larger (and deeper) one is in proximity to T_2O_7H.

without counterion are shown in Figure 2. The minima of the potential are represented by the gray lobes, and they actually overlap the most stable positions reported above for H^+. This suggests that $V_H(\mathbf{r})$ can help identifying the regions of the zeolite where the proton will tend to localize.

In order to evaluate the relative acidity of the variou sites, we have calculated the difference Δ between the total energy of T_iO_jH and that of a structure with Al in the same tetrahedral site but the proton replaced by a uniform positive background of total charge +1. This quantity differs from the deprotonation energy by an amount which does not depend on the proton site. The resulting values of Δ, reported in Table 1, show that T_2O_jH sites are in general slightly more acidic than the sites with Al in T_1 (lower values of Δ), in agreement with the experimental results of ref 24.

We have tried to find a correlation between acidity and structural properties, as done in much theoretical work on zeolites; see, e.g., refs 25, 27, and 28. In Table 2, structural parameters for the various H^+ sites are presented. We remark that T_2O_jH sites have AlO_j distances and AlO_jSi angles (both in bold characters) that are larger than those of the T_1O_jH sites. This is particularly relevant for T_2O_5H, which is the most acidic site. A larger AlO_jSi angle should correspond to a stronger *p* character and, thus, to a weakening of the O_jH bond.

TABLE 2: Structural Parameters of Protonated Sites of Offretite[a]

	Al(T1)			
	HO_1	HO_2	HO_3	HO_4
OH	1.002	1.021	1.003	1.001
SiO	1.685	1.682	1.681	1.694
AlO_1	**1.852**	1.679	1.669	1.699
AlO_2	1.681	**1.873**	1.694	1.683
AlO_3	1.678	1.686	**1.871**	1.678
AlO_4	1.704	1.688	1.678	**1.872**
AlO_1Si	**137.1**	152.5	155.6	141.3
AlO_2Si	154.9	**137.5**	149.2	145.3
AlO_3Si	153.3	143.2	**136.6**	149.4
AlO_4Si	141.2	145.9	150.2	**136.8**
AlOH	107.8	108.7	107.5	107.7

	Al(T2)		
	HO_5	HO_6	HO_7
OH	1.015	1.004	1.002
SiO	1.698	1.693	1.692
AlO_4	1.703	1.683	1.692
AlO_5	**1.936**	1.706	1.703
AlO_6	1.682	**1.905**	1.685
AlO_7	1.681	1.683	**1.889**
AlO_4Si	138.7	153.1	150.4
AlO_5Si	**159.4**	176.0	169.0
AlO_6Si	146.6	**142.5**	157.9
AlO_7Si	141.8	153.1	**138.6**
AlOH	93.8	104.6	108.8

[a] Bond lengths in Å; angles in deg.

B. Dynamical Properties. The basic features of the vibrational spectra of zeolites can be understood by considering the normal modes of a TO_4 (T = Si, Al) tetrahedron and of a TOT unit.[29] In TO_4, there are four normal modes: the simply degenerate (A_1) symmetric stretching, the antisymmetrical 3-fold degenerate (T_2) stretching, the 3-fold degenerate (T_2) bending, and the 2-fold (E) degenerate bending. For TOT, the three normal modes comprise symmetric and asymmetric stretching and a bending mode. It turns out that in zeolites, the coupling through oxygen (between two tetrahedra) is larger than within tetrahedra. Thus, the spectrum of stretching modes is formed by two bands arising from the TOT, each of which is further split into a A_1 band and a T_2 band. Experimentally the infrared spectra of zeolites can be subdivided in four regions: asymmetric stretching, at frequencies of 1000−1250 cm^{-1}; symmetric stretching, at 700−850 cm^{-1}; bending modes, at 250−500 cm^{-1}; and cation-related modes, below 200 cm^{-1}.

To study the vibrational spectrum of protonated offretite, we have carried out a dynamical (microcanonical) simulation of ∼0.9 ps at $T \sim 480$ K, with the proton initially located at T_2O_7H (its most stable binding site). In these calculations, the LDA was used. In Figure 3, the displacement for each atomic species in our system is plotted as a function of the simulation time. The corresponding mean-square displacements are given in Table 3. As expected, the proton undergoes the largest displacements in the course of the simulation. Despite such displacements, the proton remains always localized on the same oxygen. In fact, experimental estimates of the energy barrier required for the proton to hop from one site to the other are relatively large (∼10−14 kcal/mol); see, e.g., ref 30.

The vibrational spectrum of offretite has been evaluated by performing the Fourier transform of the atomic velocity autocorrelation function.[31] This spectrum is plotted in Figure 4a, while the Figure 4b we show the spectrum of vibrations localized on the proton. As our simulation is rather short, only a qualitative analysis is possible. At 1160 and 1040 cm^{-1}, the

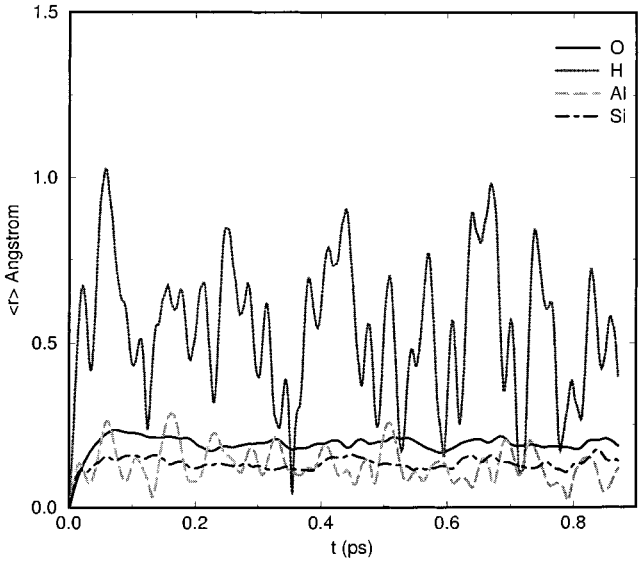

Figure 3. Displacement of each atomic species from its equilibrium position during a dynamical simulation at $T \sim 480$ K, in protonated offretite with H^+ in T_2O_7H. The curves for O and Si are averaged over all atoms of this type.

TABLE 3: Root-Mean-Square Displacements ⟨r⟩ (in Å) in Protonated Offretite during a Dynamical Simulation at 480 K[a]

	atoms			
	H	O	Al	Si
⟨**r**⟩	0.212 ± 0.014	0.011 ± 0.001	0.045 ± 0.001	0.015 ± 0.001

[a] For O and Si, averages over all atoms of these species were taken. Errors were evaluated by comparing values of ⟨**r**⟩ in different sections of the run.

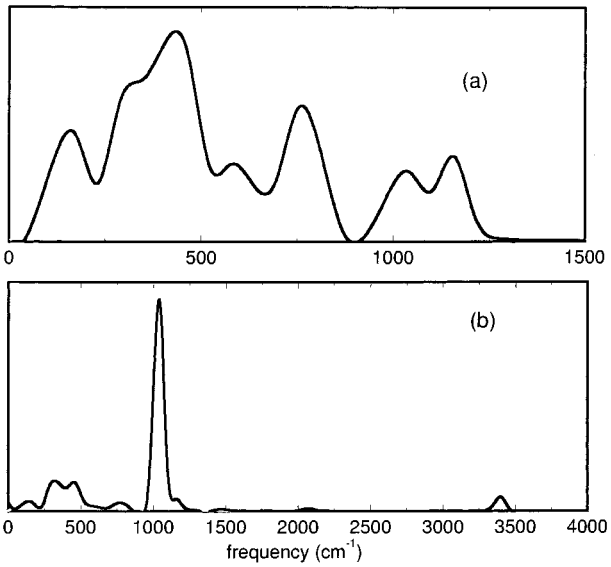

Figure 4. Vibrational spectrum at $T \sim 480$ K, obtained from the Fourier transform of the velocity autocorrelation function, in protonated offretite with H^+ in T_2O_7H. (a) Spectrum of vibrations of both the framework and the proton. (b) Spectrum of vibrations localized on the proton. Note the different frequency scales of a and b.

bands of the asymmetric stretching can be seen, while the bands at 560 and 750 cm^{-1} correspond to the symmetric stretching modes. The results are in good agreement with experimental spectra for offretite, which show absorption bands at 1155, 1040, 790, and 600−650 cm^{-1}.[32] The peaks at 170, 300, and 405 cm^{-1} in the theoretical spectrum of Figure 4a arise from the bending modes.

TABLE 4: OH Stretching Frequencies Calculated for Three Different H^+ Sites of Protonated Offretites Containing either One or Three Al Atoms per Unit Cell

	frequency, cm^{-1} (0.1 ps)	
site	1 Al/cell	3 Al/cell
T_1O_3H	3503	3494
T_2O_6H	3490	3509
T_2O_7H	3525	3529

Experimental studies of OH stretching frequencies in ion-exchanged synthetized offretite have led to the identification of four bands.[33] The highest, at 3740 cm^{-1}, corresponding to a largely accessible and nonacidic OH, was assigned to a terminal group; one at 3660 cm^{-1} was found to correspond to an inaccessible and little acidic OH, possibly located in the hexagonal prism; one at 3610 cm^{-1}, largely accessible and acidic, was attributed to OH groups located in the channel; and the lowest, at 3550 cm^{-1}, also acidic but little accessible, was suggested to originate from a OH possibly located in the cancrinite cage. In order to evaluate how the OH stretching frequency is affected by the location of the proton, we performed three independent short (∼0.1-ps) simulations for a proton in three different sites: T_1O_3H (inside the cancrinite cage) and the two sites of lowest energy, i.e., T_2O_6H and T_2O_7H (the highly acidic T_2O_5H site was not considered because its energy was too high). The resulting frequencies (see Table 4), of the order of 3500 cm^{-1}, are about 50−100 cm^{-1} lower than the experimental frequencies of 3610 and 3550 cm^{-1} to which they should be compared. Moreover, calculated frequencies show differences of only 20−30 cm^{-1} between the sites, i.e., about 50% smaller than in the experiment. This may be partly due to the short duration of our simulations, which does not allow for a complete equilibration of the system. However, we may remark that the frequency for T_2O_7H, corresponding to a proton in the channel, is higher than for the others, originating from OH groups either in the cancrinite cage or in the narrow 6-fold ring of gmelinite. A similar result was obtained in another short simulation where the three protons (in the same positions) plus three Al's (two in T_2 and one in T_1) were simultaneously present in the unit cell (see Table 4). The fact that the OH group in the channel has the highest frequency is in agreement with experiment and can be rationalized by noting that for O_3H and O_6H, the neighboring oxygens weaken the OH bond, thus decreasing its frequency. Analogous mechanisms to explain the OH stretching frequencies of protonated zeolites have been proposed previously.[26,27]

IV. K^+, Na^+, and Cu^+ Cations in Offretite

A. Structure and Energetics of the Various Cation Sites. In order to study the substitution of Si^{4+} by (Al^{3+}, M^+) (M^+ = K^+, Na^+, Cu^+), we replaced a Si^{4+} in a T (T_1 or T_2) site by an Al^{3+} and introduced a M^+ in a bridging position between two oxygens bonded to Al. As T_1 and T_2 have respectively 4 and 3 nonequivalent oxygens, there are 10 possible starting structures. Preliminary calculations with full geometry relaxation on these 10 structures were carried out for K^+ and Na^+, using a relatively low value for the cutoff ($E_{cut,1} = 16$ Ry).[10] These calculations allowed us to identify four low-energy sites, for which calculations using a larger basis set ($E_{cut,1} = 20$ Ry) were then carried out. Except for a few structures, a new reoptimization of atomic positions was performed with the higher cutoff of 20 Ry. These geometries have been used for further basis set convergence tests with $E_{cut,1} = 24$ Ry,[10] as well as for GGA calculations. In the case of Cu^+, the geometries obtained for Na^+ was used as a starting point for a full structural optimization

TABLE 5: Substitution Energies of Relevant Cation-Binding Sites in Offretites with One Si/(Al, M) Substitution per Unit Cell (M = Na, K, Cu)[a]

	Na^+		K^+		Cu^+	
structure	LDA	GGA	LDA	GGA	LDA	GGA
S1	−66.8 (1.2)	−68.5 (0.2)	−74.3 (0.0)	−72.9 (0.0)	−57.0 (3.9)	−46.0 (6.3)
S2	−68.0 (0.0)	−68.3 (0.4)	−69.8 (4.5)	−70.6 (2.3)	−60.6 (0.3)	−48.9 (3.4)
S3	−65.9 (2.1)	−67.5 (1.2)	−69.3 (5.0)	−72.7 (0.2)	−51.7 (9.2)	−46.7 (5.6)
S4	−67.7 (0.2)	−68.7 (0.0)	−63.0 (11.2)	−59.2 (13.7)	−60.9 (0.0)	−52.3 (0.0)

[a] S1 corresponds to an Al in T1; S2, S3, S4 to Al in T2. Values in parentheses are substitution energies relative to the most stable site.

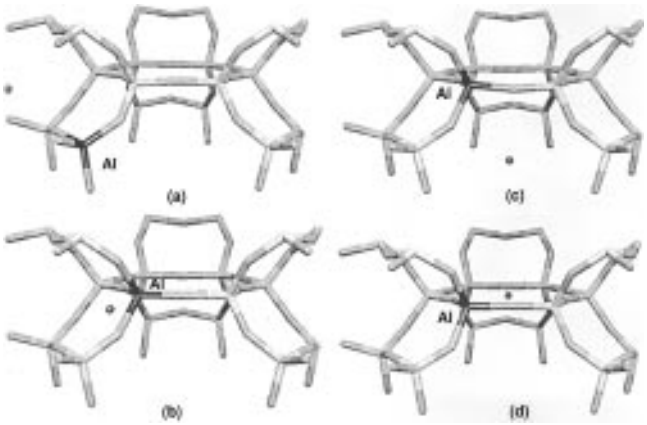

Figure 5. Structure of the four relevant binding sites for monovalent cations in offretite. (a) S1; (b) S2; (c) S3; (d) S4. All atoms within a unit cell are shown. Cations are represented by the solid spheres. For S1, the Al atom is in T_1; in all other cases, it is in T_2.

(with $E_{cut,1} = 20$ Ry). As mentioned in section II, the structures obtained at the LDA level were used for non-self-consistent GGA calculations.

The four low-energy cation sites, which we shall denote S1, S2, S3, and S4, are presented in Figure 5. For all these sites, except for S1, the Al atom is in T_2. S1 is approximately at the center of the carcrinite cage and corresponds closely to the proton site T_1O_3H, S2 is in the channel (and corresponds to T_2O_7H), S3 is close to the 8-fold window of the gmelinite cage (and corresponds to T_2O_5H), and S4 is approximately at the center of the 6-fold ring of T_2 sites of the gmelinite cage (and corresponds to T_2O_6H). The energies to substitute a Si^{4+} by (Al^{3+}, M^+) have been calculated using an expression analogous to that used for H^+. These energies, calculated both at the LDA and GGA levels, are reported in Table 5 for all three cations of interest. We can remark that differences between the LDA and GGA substitution energies are small for Na^+, for which they do not exceed 2 kcal/mol, somewhat larger for K^+, for which they are ∼4 kcal/mol, and even larger for Cu^+, for which they are of the order of 10 kcal/mol. In spite of the small differences between LDA and GGA, for Na^+, the relative ordering of sites is different in the two approximations, whereas the ordering does not change for K^+ and Cu^+. This is due to the fact that the different sites are much closer in energy in the case of Na^+ (smaller site selectivity). For K^+, the GGA leads to a greater stability of S3 and to a further destabilization of S4, whereas for Cu^+, a destabilization of S2 takes place. Within the GGA, which should yield the most accurate results, S4 at the center of the gmelinitic 6-fold ring is the most stable site for both Na^+ and Cu^+, whereas S1 inside the carcrinite cage is the most stable site for K^+. Moreover, for Na^+, there are at least two other low-energy sites, whereas for Cu^+, the site selectivity is quite pronounced. We remark that the siting preferences of Na^+ and H^+ are quite similar, while the behavior of K^+, for which steric effects are much more important, is substantially different. We also notice that substitution energies for Cu^+ are significantly smaller in absolute value than for Na^+ and K^+, indicating that Si/(Al, Cu) substitutions in offretite are less favorable than Si/(Al, K) and Si/(Al, Na) substitutions.

TABLE 6: Structural Parameters for Offretite with a Si/(Al, K) Substitution per Unit Cell[a]

	S1		S2	S3	S4
AlO_1	1.691	AlO_4	1.741	1.740	1.699
AlO_2	1.725	AlO_5	1.714	1.749	1.737
AlO_3	1.733	AlO_6	1.698	1.701	1.754
AlO_4	1.697	AlO_7	1.741	1.708	1.699
KO	2.695	KO	2.704	2.574	2.453
KO	2.885	KO	2.705	2.769	2.531
KO	2.936	KO	2.715	2.791	2.533
KO	3.003	KO	2.717		2.656
KO	3.069	KO			2.785
KO	3.277	KO			2.814
O_1AlO_2	108.6	O_4AlO_7	99.1	107.3	112.4
O_2AlO_3	102.0	O_4AlO_5	111.1	104.9	111.9
O_3AlO_4	107.5	O_5AlO_6	113.2	112.0	104.0
O_4AlO_1	112.6	O_6AlO_7	111.1	111.0	108.1

[a] Bond lengths are in Å and angles in deg. Only KO distances smaller than 3.3 Å are listed.

TABLE 7: Structural Parameters for Offretite with a Si/(Al, Na) Substitution per Unit Cell[a]

	S1		S2	S3	S4
AlO_1	1.688	AlO_4	1.749	1.758	1.701
AlO_2	1.734	AlO_5	1.707	1.742	1.733
AlO_3	1.745	AlO_6	1.696	1.700	1.761
AlO_4	1.695	AlO_7	1.749	1.701	1.701
NaO	2.304	NaO	2.356	2.204	2.222
NaO	2.421	NaO	2.356	2.252	2.310
NaO	2.782	NaO	2.343	2.410	2.413
NaO	2.827	NaO	2.343		2.564
O_1AlO_2	109.1	O_4AlO_7	97.6	109.2	110.9
O_2AlO_3	100.3	O_4AlO_5	111.7	99.6	113.2
O_3AlO_4	107.2	O_5AlO_6	114.2	111.6	98.5
O_4AlO_1	114.5	O_6AlO_7	110.2	113.2	110.2

[a] Bond lengths are in Å and angles in deg. Only NaO distances smaller than 2.85 Å are listed.

The structural parameters for the different cations and sites are reported in Tables 6−8. Some small differences with respect to our previously published results[10] are due to the fact that an higher cutoff is used in the present calculations. It appears that the number of oxygen neighbors of K^+ and Na^+ varies between two and four, whereas the coordination of Cu^+ is more clearly equal to two. Typical MO distances are 2.2−2.4, 2.6−3.0, and 1.9−2.1 Å for Na^+, K^+, and Cu^+, respectively. The 2-fold coordination of Cu^+ as well as the typical CuO distances agree with the results of the recent density functional cluster calculation.[8] The local cation-induced distortions of the zeolite framework consist of an elongation (by ∼0.04−0.10 Å) of two AlO bonds of the AlO_4 tetrahedron with respect to the other two, indicating the presence of two relatively weak MO bonds.

Experimentally, both Gard and Tait[3] and Alberti *et al.*[4] found that in hydrated natural offretite, K^+ is inside the carcrinite cage. Moreover, Mortier *et al.*[5] proposed that upon dehydration, Ca^{2+} displaces K^+ from the cancrinite cage via a process of "internal ion exchange" and that the displaced K^+ occupies the 8-fold

TABLE 8: Structural Parameters for Offretite with a Si/(Al, Cu) Substitution per Unit Cell[a]

	S1		S2	S3	S4
AlO_1	1.681	AlO_4	1.738	1.797	1.688
AlO_2	1.742	AlO_5	1.702	1.749	1.746
AlO_3	1.761	AlO_6	1.706	1.688	1.811
AlO_4	1.695	AlO_7	1.738	1.685	1.688
CuO	2.085	CuO	1.867	1.974	1.924
CuO	2.133	CuO	1.868	2.158	2.003
CuO	2.146	CuO	2.629	2.171	2.327
CuO	2.450	CuO	2.629		
O_1AlO_2	108.5	O_4AlO_7	99.4	106.8	109.0
O_2AlO_3	113.0	O_4AlO_5	113.6	101.4	114.7
O_3AlO_4	104.8	O_5AlO_6	112.8	111.1	100.9
O_4AlO_1	116.1	O_6AlO_7	108.4	112.8	108.5

[a] Bond lengths are in Å and angles in deg. Only CuO distances smaller than 2.65 Å are listed.

ring of the gmelinite cage. Consistent with experimental observations, our results for K^+ indicate that the most stable site S1 is immediately followed by S3, close to the gmelinitic 8-fold ring. We also find that for the S1 site, i.e., K^+ inside the cancrinite cage, the two closest oxygens (at distances of 2.695 and 2.885 Å; see Table 6) are of O_3 type and the two next neighbors (at distances of 2.936 and 3.003 Å) are of O_2 type, while for the S3 site, two O_4 neighbors at distances of 2.574 and 2.769 Å are present, followed by an O_5 at 2.791 Å. A comparison of these results with the available experimental data reveals a few differences. In fact, experimentally, Gard and Tait[3] found that each K^+ inside a cancrinite cage is coordinated to six O_3 at 2.96 Å and six O_2 atoms at 3.33 Å, while for K^+ at the 8-ring, Mortier *et al.* found four O_4 neighbors at 3.26 Å and two O_1 atoms slightly further away at 3.35 Å (here we use our site labeling, as given in section IIA, in which O sites are interchanged with respect to refs 3 and 5 namely, $O_1 \rightleftharpoons O_4$, $O_2 \rightleftharpoons O_3$, $O_5 \rightleftharpoons O_6$). There are two main effects which should contribute to the differences between theory and experiment. The first effect is the different Al:Si ratio: in the experimental samples, approximately five Al atoms per unit cell are present, whereas in our calculations, there is one Al/unit cell only. This difference is likely to be responsible for the fact that the calculated KO distances appear to be somewhat shorter than the experimental ones. The second effect is that while in our calculations *all* unit cells always have the Al atom at the *same* site (because of the periodic boundary conditions), in reality, Al atoms are randomly distributed among available T sites and their positions in different cells are obviously different. This leads to an averaging effect which could explain why the observed coordination of K^+ is higher and more symmetrical than that found in the calculations.

B. Dynamical Properties of Na−Offretite. We have studied the dynamical properties of offretite in the presence of a Na^+ cation at S2, by means of a dynamical simulation of duration ~2 ps in which the temperature was raised from $T \sim$ 300 K to $T \sim$ 820 K. In Figure 6, the displacements of the different atoms in the course of this simulation are displayed, while the corresponding mean-square displacements are given in Table 9. The average displacements of Na^+ are larger than those of the other atoms, because it is not part of the zeolite framework. The vibrational spectrum of offretite at 820 K is shown in Figure 7a, while that in Figure 7b refers to the vibrations localized in Na^+.

The general features of the spectrum in Figure 7a are the same as for protonated offretite (in Figure 4a). At 1120 and 1025 cm^{-1}, the peaks of the asymmetric stretching are found, while at 790 and ~600 cm^{-1} we can see the bands for the symmetric stretching. Between 200 and 500 cm^{-1}, there are

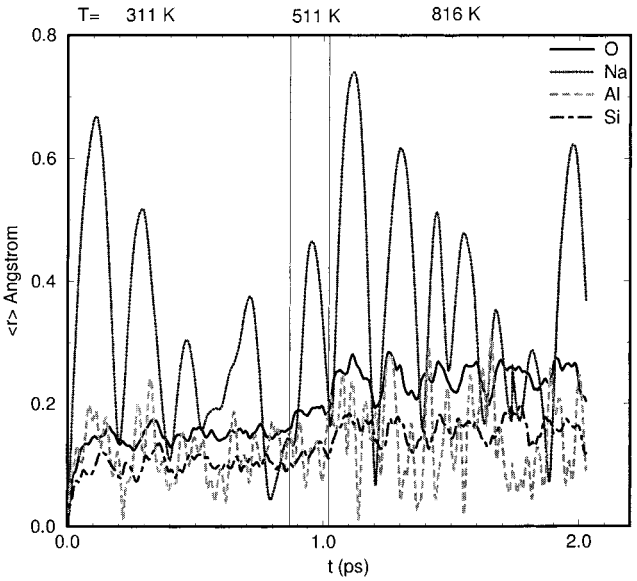

Figure 6. Displacement of various atomic species from their equilibrium positions during a dynamical simulation for offretite with one Al^{3+} replacing Si^{4+} in T_2 and one Na^+ in S2. Temperatures are indicated on the graph. The curves for O and Si are averaged over all atoms of this type.

TABLE 9: Root-Mean-Square Displacements ⟨r⟩ (in Å) in Offretite with One Si/(Al, Na) Substitution per Unit Cell during Dynamical Simulations at 311 and 816 K[a]

	atom			
⟨r⟩	Na	O	Al	Si
311 K	0.159 ± 0.041	0.010 ± 0.003	0.043 ± 0.009	0.013 ± 0.004
816 K	0.171 ± 0.018	0.021 ± 0.002	0.068 ± 0.000	0.018 ± 0.000

[a] For O and Si, averages over all atoms of these species were taken. Errors were evaluated by comparing values of ⟨r⟩ in different sections of the run.

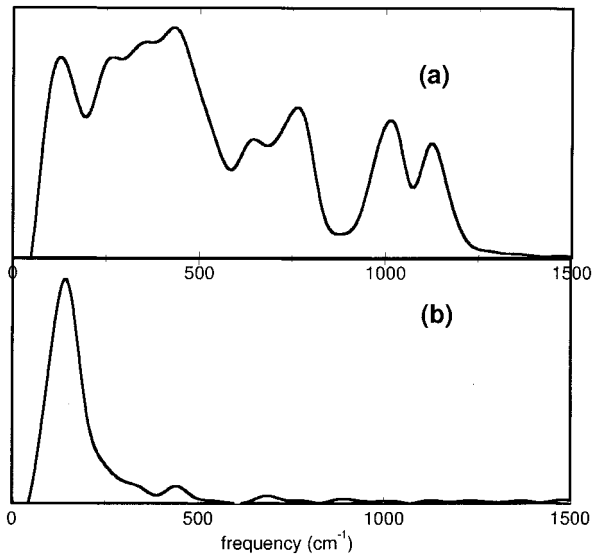

Figure 7. Vibrational spectrum at $T \sim$ 480 K, obtained from the Fourier transform of the velocity autocorrelation function, in offretite with Na^+ in S2. (a) Spectrum of vibrations of both the framework and Na^+. (b) Spectrum of vibrations localized on Na^+.

three bands corresponding to the bending modes. Motions localized on the cation are peaked at 145 cm^{-1}.

C. Influence of the Al/Si Ratio and M^+-M^+ Interactions on Cation Siting. Offretites usually have an Al/Si ratio corresponding to more than one Al per unit cell, add it is therefore interesting to examine this possibility as well. For

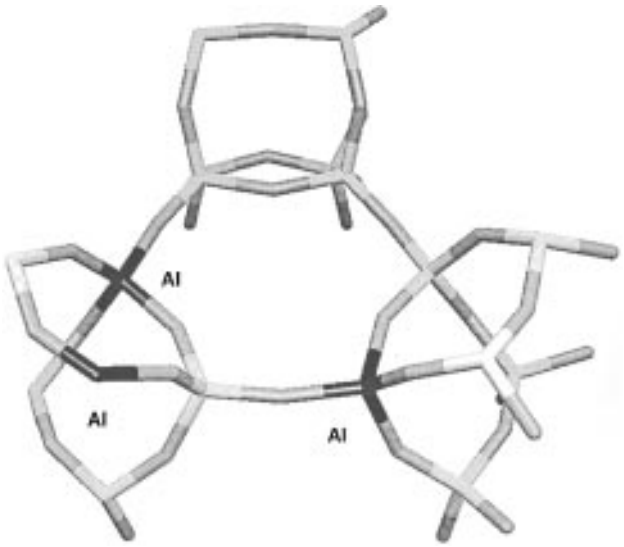

Figure 8. Structure ($2T_1$, $1T_1$), with three Al's per unit cell.

these cases, however, finding the most stable structure is much more difficult than in the case of a single Al/unit cell, because the number of possibilities to distribute the Al atoms among the different sites is extremely high. In the present study, we are restricted to a well-defined choice and have considered two Al's in T_2 sites plus one Al in a T_1, as depicted in Figure 8. The choice of this distribution, which we shall denote ($2T_2$,-$1T_1$), can be justified by the greater stability of T_2 with respect to T_1. We remark, however, that this distribution does not obey the so-called "extended Löwenstein rule" (i.e., the distances between the Al's are not the largest distances compatible with the chosen Al:Si ratio) so that other configurations with two Al's in T_2 and one in T_1 might actually be more stable.

Using the Al distribution of Figure 8, three Na^+ ions have been added at positions S1, S2, and S4, as suggested by the results obtained for the case of a single Al/unit cell. After a structural relaxation, a dynamical simulation was started, by heating the system first to 150 K and next to 500 K. In the initial heating, the Na^+ at S2 moved by a few angstrom to a new position, which we shall denote S2′, where it remained for the rest of the simulation (of ∼1.4 ps). In Figure 9, the atomic displacements for the various species are plotted as a function of the simulation time. The initial displacement of one of the Na^+ cations is apparent. The root-mean-square displacement $\langle \mathbf{r} \rangle$ of the Na^+ cations in the new equilibrium structure is 0.201 ± 0.036 Å at 500 K, i.e., a value of the same order as that obtained in the case of a single Si/(Al, Na) substitution per cell.

The migration of Na^+ from S2 to S2′ suggests a greater stability of the new site. After relaxation, we indeed find that the new structure is as much as 14 kcal/mol lower in energy than our initial guess, which was based on the results for the case of one Al/unit cell. The electrostatic potential V_H for the ($2T_2$, T_1) structure of Figure 8, prior to introduction of the three Na^+ counterions, is shown in Figure 10. Three minima can be seen, two of which are close to cation positions S1 and S4. The third pocket of V_H is close neither to S2 nor to S2′, indicating that the choice of the final position S2′ is influenced also by cation−cation interactions (not contained in V_H).

V. Summary and Conclusions

In this paper, we have presented a theoretical study of the structure, energetics, and dynamical properties of offretite under different $Si^{4+}/(Al^{3+}, M^+)$ substitutions, $M^+ = H^+$, Na^+, K^+, Cu^+. Our study employs density functional theory both at the

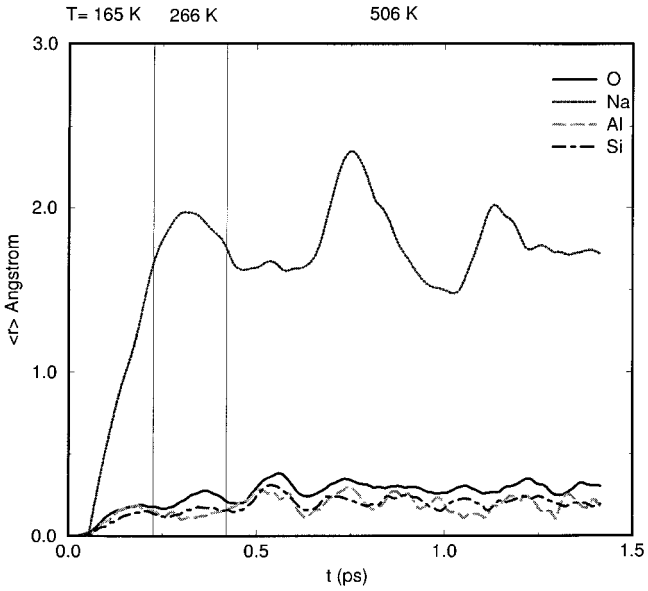

Figure 9. Displacement of each atomic species from its equilibrium position during a dynamical simulation in offretite with three $Si^{4+}/(Al^{3+}, Na^+)$ substitutions/cell. The three Na^+ are initially in S1, S2, and S4. All curves are averaged over all atoms of each type.

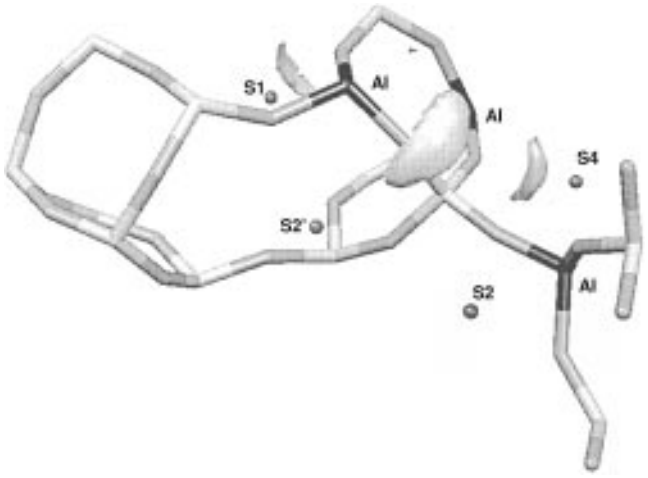

Figure 10. Isovalue surfaces of the electrostatic potential (−0.139 au) of offretite with three Al's in ($2T_2$, T_1), as shown in Figure 8, and no counterion. The sites of the three Na^+ cations in the simulation of Figure 9 are also shown. S2′ is the final position of the Na^+ cation initially in S2 (see text).

LDA and GGA levels, and takes into account the full periodicity of the lattice. Most of our calculations have been done for a single $Si^{4+}/(Al^{3+}, M^+)$ substitution per unit cell, while a limited set of computations have been carried out for the case of three substitutions per cell.

Our results show that cation siting in zeolites depends remarkably on the nature of the counterion. For H^+, and to a lesser extent also for Na^+, the preferred sites correspond to the lowest minima of the electrostatic potential calculated in the absence of the counterions. For K^+, steric effects are important so that an interpretation based only on the lowest minima of this potential no longer holds. While H^+ is always singly coordinated and induces significant local deformations of the lattice, Cu^+ is found to prefer 2-fold coordination, and Na^+ and K^+ have coordination between two and four. As CuO bonding distances are shorter than NaO and KO distances, we infer that Cu^+ is more tightly bound than Na^+ and K^+. In agreement with experiments, we also find that the T_2 site for Al is more stable than T_1, that in the presence of H^+, T_2 is more acidic than T_1, and that for K^+, two sites very close in energy occur,

the lowest being inside the cancrinite cage and the other near the 8-fold gmelinitic ring. Moreover, our results show taht cation siting, i.e., the relative stability of different sites, is affected by the Al/Si ratio as well as by the mutual interactions between the cations.

The vibrational spectrum of the framework that we have derived from our dynamical simulations agrees quite well with those of the available experiments. Calculated OH stretching frequencies show a weaker dependence of the H^+ position with respect to that found in experiments. The reason of this is not completely clear, even if it could in part be due to the inaccuracies of our calculations. In agreement with experiment, we find, however, that more "open" positions (e.g., in the channel) have somewhat higher frequencies than sites within cages or rings. Here the presence of nearby oxygens may weaken the OH bond, thus lowering its frequency.

Acknowledgment. Calculations were run on the Nec-SX3 and Nec-SX4 of the CSCS at Manno, Switzerland. We thank A. Pasquarello for useful discussions and help in the GGA calculations. This work was financially supported by the Swiss National Foundation (Project No. 20-41830.94) and the Swiss OFES as part of the European COST D3 action.

References and Notes

(1) For a general review, see, e.g.: *Modelling of Structure and Reactivity in Zeolites*; Catlow, C. R. A., Ed.; Academic: New York, 1992.
(2) See, e.g.: Dyer, A. *An Introduction to Zeolite Molecular Sieves*; John Wiley and Sons: Chichester, 1988.
(3) Gard, J. A.; Tait, J. M. *Acta Crystallogr*. **1972**, *B28*, 825.
(4) Alberti, A.; Cruciani, G.; Galli, E.; Vezzalini, G. *Zeolites* **1996**, *17*, 457.
(5) Mortier, W. J.; Pluth, J. J.; Smith, J. V. *Z. Kristallogr*. **1976**, *143*, 319.
(6) Whyte, T. E.; Wu, E. L.; Kerr, G. T.; Venuto, J. R. *J. Catal*. **1971**, *20*, 88.
(7) Aiello, R.; Barrer, R. M.; Davies, J. A.; Kerr, I. S. *J. C. Chem. Soc., Faraday Trans*. **1970**, *66*, 1610.
(8) See, e.g.: Trout, B. L.; Chakraborty, A. K.; Bell, A. T. *J. Phys. Chem*. **1996**, *100*, 17582 and references therein.
(9) Campanan, L.; Selloni, A.; Weber, J.; Pasquarello, A.; Papai, I.; Goursot, A. *Chem. Phys. Lett*. **1994**, *226*, 245.
(10) Campana, L.; Selloni, A.; Weber, J.; Goursot, A. *J. Phys. Chem*. **1995**, *99*, 16351.
(11) Car, R.; Parrinello, M. *Phys. Rev. Lett*. **1985**, *55*, 2471.
(12) The name GGA is generally used to indicate the approximation developed by Perdew and Wang, reported in: Perdew, J. P.; Chevary, J. A.; Vosko, S. H.; Jackson, K. A.; Pederson, M. R.; Singh, D. J.; Fiolhais, C. *Phys. Rev. B* **1992**, *46*, 6671.
(13) See, e.g.: Dal Corso, A.; Pasquarello, A.; Baldereschi, A.; Car, R. *Phys. Rev. B* **1996**, *53*, 1180 and references therein.
(14) For a recent review, see: Galli, G.; Pasquarello, A. *Computer Simulations in Chemical Physics*; Allen, M. P., Tildesley, D. J., Eds.; Kluwer: Dordrecht, 1994; pp 261−313.
(15) Bachelet, G. B.; Hamann, D. R.; Schlüter, M. *Phys. Rev. B* **1982**, *26*, 4199.
(16) Kleinman, L.; Bylander, D. M. *Phys. Rev. Lett*. **1982**, *48*, 1425.
(17) Vanderbilt, D. *Phys. Rev. B* **1990**, *41*, 7892.
(18) Laasonen, K.; Pasquarello, A.; Car, R.; Lee, C.; Vanderbilt, D. *Phys. Rev. B* **1993**, *47*, 10142.
(19) Perdew, J. P.; Zunger, A. *Phys. Rev. B* **1981**, *23*, 5048.
(20) Hammer, B.; Jacobsen, K. W.; Norskov, J. K. *Phys. Rev. Lett*. **1993**, *70*, 3971.
(21) Tassone, F.; Mauri, F.; Car, R. *Phys. Rev. B* **1994**, *50*, 10561.
(22) Blochl, P. *Phys. Rev. B* **1994**, *50*, 17953.
(23) Chauvin, B.; Boulet, M.; Massiani, P.; Fajula, F.; Figueras, F.; Des Courieres, T. *J. Catal*. **1990**, *126*, 532.
(24) Barthomoeuf, D. *Mater. Chem. Phys*. **1987**, *17*, 49.
(25) Sauer, J. *Chem. Rev*. **1989**, *89*, 199.
(26) Jacobs, P. A.; Mortier, W. J. *Zeolites* **1982**, *2*, 226.
(27) Kramer, G. J.; van Santen, R. A. *Chem. Rev*. **1995**, *95*, 637.
(28) Redondo, A.; Hay, P. J. *J. Phys. Chem*. **1993**, *97*, 11754.
(29) van Santen, R. A.; Vogel, D. L. *Adv. Solid-State Chem*. **1989**, *1*, 151−224.
(30) Sarv, P.; Tuherm, T.; Lippmaa, E.; Keskinen, K.; Root, A. *J. Phys. Chem*. **1995**, *99*, 13763.
(31) Allen, M. P.; Tildesley, D. J. *Computer Simulation of Liquids*; Oxford Science Publications, Clarendon: Oxford, 1987.
(32) Mirodatos, C. Modification des propriétés des zéolithes Y et offretites par échange cationique. Thèse d'Etat, Université Claude Bernard, Lyon, 1977.
(33) Mirodatos, C.; Abou-Kais, A.; Vedrine, J. C.; Barthomeuf, D. *J. Chem. Soc., Faraday Trans*. **1978**, *74*, 1786.